Scaling Effect on the Relationship between Landscape Pattern and Land Surface Temperature: A Case Study of Indianapolis, United States

Hua Liu and Qihao Weng

Abstract

The objective of this paper is to examine the scaling-up effect on the relationship between landscape patterns and land surface temperatures based on a case study of Indianapolis, United States. The integration of remote sensing, GIS, and landscape ecology methods was used in this study. Four TERRA ASTER images were acquired to derive the land-use and land-cover (LULC) patterns and land surface temperatures (LST) in different seasons. Each LULC and LST image was resampled to eight spatial scales: 15, 30, 60, 90, 120, 250, 500, and 1,000 m. The scaling-up effect on the spatial and ecological characteristics of landscape patterns and LSTs were examined by the use of landscape metrics. Optimal spatial resolutions were determined on the basis of the minimum distance in the landscape metric spaces. The results show that the patch percentages of LULC and LST patches were not strongly affected by the scaling-up process in different seasons. The patch densities and landscape shape indices and LST patches kept decreasing across the scales without distinct seasonal differences. Thirty meters was found to be the optimal resolution in the study of the relationship between urban LULC and LST classes. Ninety meters was found to be the optimal spatial resolution for assessing the landscape-level relationship between LULC and LST patterns. This paper may provide useful information for urban planners and environmental practitioners to manage urban landscapes and urban thermal environments as a result of urbanization.

Introduction

Scale influences the examination of the landscape patterns in a region. The change of scale is relevant to the issues of data aggregation, information transfer, and the identification of appropriate scales for analysis (Krönert *et al.*, 2001; Wu and Hobbs, 2002). Extrapolation of signals across spatial scales is a necessary research task (Turner, 1990). It is believed that spatial characteristics could be transferred across scales under specific conditions (Allen *et al.*, 1984). Therefore, we need to know how the information is transferred from a fine scale to a broad scale (Krönert *et al.*, 2001). In remote sensing studies, choosing various satellite sensors may result in different research results, since they usually have different spatial resolutions. Therefore, it is significant to examine the changes in spatial configuration of any landscape pattern as a result of different spatial resolutions of satellite imagery. Moreover, it is always necessary to find the optimal scale(s) for the study in which the environmental processes operate.

Land-use and land-cover (LULC) pattern is regarded as an important determinant of ecosystem function, and can be considered as the representative of landscape pattern in an *in situ* area (Bain and Brush, 2004). LULC categories are linked to distinct behaviors of urban thermal environment (Voogt and Oke, 1997). Solar radiation and land surface temperature (LST) are important parameters for analysis of urban thermal behavior (Aguiar *et al.*, 2002). LST reflects the result of surface-atmosphere interactions and energy fluxes between the ground and the atmosphere on the Earth (Wan and Dozier, 1996). Research is therefore needed to examine the relationship between LULC and LST (Weng *et al.*, 2004; Weng *et al.*, 2006). Furthermore, seasonal changes may have major impact on soil moisture and tree canopy components, and thus on the LULC-LST relationship. However, little research has so far been done to examine the scaling-up effect on the relationship between landscape pattern and LST.

Landscape/LULC patches in a region may have different sizes, shapes and spatial arrangements, which contribute to the spatial heterogeneities of the landscape. In order to understand the dynamics of patterns and processes and their interactions in a heterogeneous landscape (such as the urban areas commented on by the authors), one must be able to accurately quantify the spatial pattern and its temporal changes of the landscape (Wu *et al.*, 2000). In recent years, a series of landscape metrics have been developed to characterize the spatial patterns of landscapes and to compare ecological quality across the landscapes (McGarigal and Marks, 1995; Gustafson, 1998). However, there is lack of

Hua Liu is with the Department of Political Science and Geography, Old Dominion University, Norfolk, VA, 23529, and formerly with the Center for Urban and Environmental Change, Department of Geography, Geology, and Anthropology, Indiana State University, Terre Haute, IN 47809.

Qihao Weng is with the Center for Urban and Environmental Change, Department of Geography, Geology, and Anthropology, Indiana State University, Terre Haute, IN 47809 (qweng@indstate.edu).

Photogrammetric Engineering & Remote Sensing
Vol. 75, No. 3, March 2009, pp. 291–304.

0099-1112/09/7503–0291/$3.00/0

published works on the application and sensitivity analysis of landscape metrics in the study of the relationship between LULC and LST patterns. In this study, a method was developed to identify the scaling effect on the relationship between the LULC and LST patterns by the use of landscape metrics. LULC and LST information in four seasons in Indianapolis was derived from ASTER imagery. The scaling-up effect on the spatial characteristics of LULC and scaling-up and -down effect on LST were then examined based on the analysis of class-based landscape metrics. The similarity in their landscape structures were determined based on the minimum distance in the landscape metric space in order to determine the optimal resolution for studying the urban thermal landscape.

The Issue of Scale

The theories, models, and procedures for scaling are crucial to understand heterogeneous landscapes (Wu and Qi, 2000; Wu and Hobbs, 2002). Methods and technologies have become more and more important for the examination of spatial arrangements at wide spatial scales. Regionalization describes a transition from one (micro-, meso-, or macro-) scale to another. Up-, down-scaling is a fundamental operation of transition (Krönert *et al.*, 2001).

Spatial resolution has been a focus in remote sensing studies. It is necessary to estimate the capability of remote sensing data in landscape mapping since the application of remote sensing may be limited by its spatial resolution (Aplin, 2006; Buyantuyev and Wu, 2007; Ludwig *et al.*, 2007). Imagery with finer resolution includes greater spatial information, which, in turn, enables the description of smaller features than imagery with lower spatial resolution. The proportion of mixed pixels is expected to increase as spatial resolution becomes lower (Aplin, 2006). Stefanov and Netzband (2005) identified weak positive and negative correlations between NDVI and landscape structure at different spatial resolutions: 250 m, 500 m, and 1000 m when they examined the capability of MODIS NDVI data in the assessment of arid landscape characteristics for the metropolitan Phoenix. Asner *et al.* (2003) examined the significance of sub-pixel estimates of biophysical structure with the help of high-resolution remote sensing imagery, and found a strong correlation between the senescent and unmixed green vegetation cover values in a deforested area. Adaptive choice of spatial and categorical scales in landscape mapping was demonstrated by Ju *et al.* (2005). They provided a data-adaptive choice of spatial scale varying by location jointed with categorical scale by the assistance of a statistical finite mixture method. Agam *et al.* (2007) sharpened the coarse-resolution thermal imagery to finer resolution imagery based on the analysis of the relationship between vegetation index and LST. The results showed that the vegetation index based sharpening method was a significant way to improve the spatial resolution of thermal imagery.

Buyantuyev and Wu (2007) systematically analyzed the effects of thematic resolution on landscape pattern analysis. The researchers considered that two problems needed attention in landscape mapping: the multiplicity of classification schemes and the level of detail of a particular classification. They found that the thematic resolution had obvious effects on most of the landscape metrics which indicates that changing thematic resolution may significantly affect the detection of landscape changes. However, increasing the spatial resolution may not lead to a better observation since objects may be over-sampled and their features may vary and be confusing (Hsieh *et al.*, 2001; Aplin and Atkinson, 2004). Although coarse resolution may include fewer features, imagery with too fine resolution for specific purpose can be degraded in the process of image resampling (Ju *et al.*, 2005). Remote sensing data may not be always be sufficient when specific problems were addressed at specific scales and on-ground assessment may need to be evolved for more details since low-resolution remote sensing imagery cannot provide sufficient information about the location and connectivity for specific areas (Ludwig *et al.*, 2007).

LST has been used as an important indicator to evaluate urban atmosphere and to model urban climate (Voogt and Oke, 1997; Jacob *et al.*, 2002; Voogt and Oke, 2003). It is believed to be able to measure the urban heat islands' parameters, such as magnitudes, spatial extents, central positions, and directions of heat movements (Streutker, 2002 and 2003). LST has also been used in the analysis of temperature-vegetation abundance relationship, drought evaluation, modeling of urban surface temperatures with surface structural information, and forest regeneration detection (Boyd *et al.*, 1996; Voogt and Oke, 1997; McVicar and Jupp, 1998; Wan *et al.*, 2004; Weng *et al.*, 2004). Remote sensing thermal infrared (TIR) data have been widely used to retrieve LST (Luvall and Holbo, 1991; Quattrochi and Ridd, 1998; Quattrochi and Luvall, 1999; Weng *et al.*, 2004). Research has been developed to examine the scaling effect in LST retrieval (Liu *et al.*, 2006). This research retrieved LSTs from ASTER and MODIS imagery for part of the Loess Plateau in China and then scaled ASTER data to 1 km. The results showed that the accuracy of LST measurement was the major uncertainty in the study, and the variation in the LST was reduced after scaling. However, different scaling methods and terrain conditions did not show significant influence on the variation for the study area. For areas with obvious elevation changes, terrain correction could result in a significant improvement in LST measurement with the assistant of DEM analysis.

Numerous landscape metrics have been developed to quantify landscape patterns in various scales (Turner, 1990; McGarigal and Marks, 1995; Gustafson, 1998). However, it remains difficult to interpret metrics due to the poor understanding of their functions and limitations (Pickett *et al.*, 1994; Li and Wu, 2004). The landscape metrics are believed to be sensitive to spatial scales (Turner, 1990; Wang *et al.*, 1999). However, few studies have used landscape metrics in the analysis of LST configurations, not to speak of the relationship between landscape and LST patterns. On the other hand, some studies have documented the optimal spatial resolution in environmental studies (Curran and Atkinson, 1998; Petit and Lambin, 2001; Chen *et al.*, 2004; Weng *et al.*, 2004). Weng *et al.* (2004) estimated the relationship between LST and vegetation fraction in Indianapolis by using Landsat ETM+ data. The results indicated that LST possessed a slightly stronger negative correlation with green vegetation than with NDVI for all landscape pattern types crossing the scale from 30 m to 960 m, and that 120 m spatial resolution was found to be the operational scale of LST, vegetation, and NDVI images since the negative correlations reached highest at the resolution. This study intends to develop a logical method to determine an optimal resolution for examining the relationship between landscape and LST patterns on the basis of a minimum distance in the landscape metric space for the study area. This study also indicates the best resolution to study the urban area and which sort of information would be lost by choosing a particular resolution.

Study Area

The City of Indianapolis, located in Marion County, Indiana (Figure 1), is the nation's twelfth largest city, with approximately 0.8 million population (over 1.6 million in the

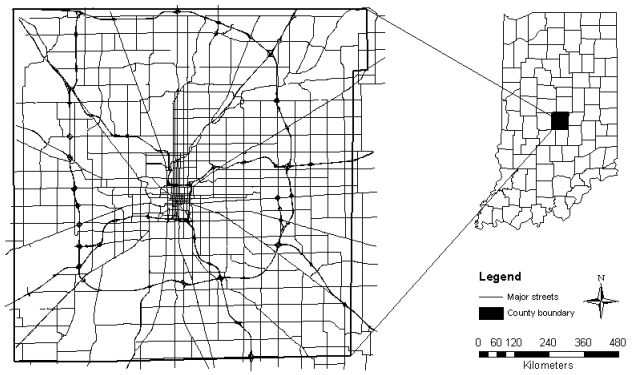

Figure 1. Study area: Indianapolis, Indiana.

metropolitan area). It lies in the middle continental region, with the highest elevation of 219 meters and a land area of 936 square kilometers. Situated in the middle of the country, Indianapolis possesses several other advantages that make it an appropriate choice. It has a single central city, and other large urban areas in the vicinity have not influenced its growth. The city is located on a flat plain, and is relatively symmetrical, having possibilities of expansion in all directions. Like most American cities, Indianapolis is increasing in population and in area. The area expansion is through encroachment into the adjacent agricultural and non-urban land. Certain decision-making forces have encouraged some sectors of Metropolitan Indianapolis to expand faster than others. Detecting and analyzing its urban thermal landscape is important for assessing and planning the city's future development.

The city has a temperate climate without pronounced wet or dry seasons. However, obvious seasonal changes can be found in the area. Its annual average temperature is 11.3°C, and the average temperature in January reaches −3.3°C and 23.9°C in July. The average annual precipitation is 1.01 meters, and about 0.06 meters in January and 0.12 meters in July. Monthly average snowfall is 0.17 meters in January. The average wind speeds are slightly higher in spring and winter than in summer and fall seasons. The average relatively humidity for the whole year does not show obvious seasonal changes.

Data and Methods

Data Preparation

Advanced Spaceborne Thermal Emission and Reflection Radiometer (ASTER) L1B and L2 images were used to derive LULC types, surface emissivity, and LSTs for the study area. The ASTER sensor collects images in 14 bands: three visible bands (15 m spatial resolution), six near-infrared bands (30 m spatial resolution), and five thermal infrared bands (90 m spatial resolution) (ASTER production description 2005). All images were acquired around 1700 GMT time with less than 10 percent cloud cover. The images were geo-corrected to the Universal Transverse Mercator (UTM) projection with NAD27 Clarke 1866 Zone 16, by using 1:24 000 Digital Raster Graphic (DRG) maps as the reference data. Approximately 40 to 50 ground control points were chosen for each image (Table 1). The root mean square errors (RMSEs) for the geo-correction were all no greater than 0.5 pixel.

LULC Classification

Nine ASTER visible and near-, middle-infrared bands (VNIR and SWIR) were used to derive six LULC types for the study area. Table 2 provides a detailed description of the LULC types. Principle component analysis was applied to choose spectrally representative bands for every single image. Unsupervised classification method (Iterative Self-Organizing Data Analysis) was then applied to group individual image into 120 clusters with the maximum iterations of 30. Each of the clusters was labeled to one of the six LULC categories in reference to 2003 and 2005 aerial photos covering the study area. Due to spectral mixture, a number of clusters were not able to be assigned to single LULC type. These spectrally mixed pixels were separated from the original image, and were then reclassified and labeled by the use of the same classification procedure as above. Re-classification continued until all spectral clusters were assigned to single LULC class. At the end, all portions of the classified image were merged to form an entire classified map. A post-classification smoothing process was executed to improve the accuracy of image classification by operating a 3×3 moving window across the images. An aerial photo was used to further improve the classification accuracy in the image refinement processing. Accuracy assessment was conducted to evaluate

Table 2. Six LULC Categories were Used to Show the Land-cover in the Study Area, City of Indianapolis, Indiana

Categories	Descriptions
Urban	Industrial lands, roads and rails, commercial, right-of-way, golf courses, soccer and recreation areas, towers, and so on
Forest	Successional stage, like pre-forest stage and mature or high canopy stage, andso on
Grassland	Prairies, pasture, savannahs, historic grasslands, farm bill program lands, caves, and subterranean features, and so on
Agriculture	Row crop by type, cereal grains,vineyards, feedlots, residue management, and confined operations, and so on
Water	Lake Michigan, rivers and streams by order and watershed, miles of unimpounded rivers and streams, and so on
Barren land	Active mine-lands, active quarries, bare dunes, and so on

Table 1. Four ASTER Images at Different Seasons were Geo-corrected to UTM System, 1866 NAD27, Zone 16 North, based on the DRG Maps. The Means and Standard Deviations of LSTs for Four Maps were Calculated

Seasons	Acquisition dates	Acquisition time (GMT)	Mean LST (°C)	Standard deviation
Winter	06 February 2006	16:45:36	−0.52	1.32
Spring	05 April 2004	16:46:39	19.06	3.24
Summer	16 June 2001	16:55:29	33.95	4.95
Fall	03 October 2000	17:00:51	28.5	3.04

TABLE 3. FOUR IMAGES WERE CLASSIFIED TO SIX CATEGORIES INDIVIDUALLY BY THE USE OF UNSUPERVISED CLASSIFICATION METHOD AND IMAGE REFINEMENT PROCESSING

Date	Categories	Reference totals	Classified totals	Number correct	Producer's accuracy (%)	User's accuracy (%)	Overall accuracy (%)	Overall kappa statistics
06 Feb 2006	Urban	52	50	42	80.77	84.00	87.33	0.85
	Forest	55	50	40	72.73	80.00		
	Grassland	54	50	44	81.48	88.00		
	Agriculture	50	50	47	94.00	94.00		
	Water	46	50	46	100.00	92.00		
	Barren land	43	50	43	100.00	86.00		
	Total	300	300	262				
05 Apr 2004	Urban	52	50	46	88.46	92.00	92.00	0.90
	Forest	50	50	46	92.00	92.00		
	Grassland	57	50	47	82.46	94.00		
	Agriculture	48	50	48	100.00	96.00		
	Water	51	50	47	90.16	94.00		
	Barren land	42	50	42	100.00	84.00		
	Total	300	300	276				
16 Jun 2001	Urban	59	50	48	81.36	96.00	88.33	0.86
	Forest	49	50	42	85.71	84.00		
	Grassland	56	50	44	78.57	88.00		
	Agriculture	48	50	45	93.75	90.00		
	Water	47	50	45	95.74	90.00		
	Barren land	41	50	41	100.00	82.00		
	Total	300	300	265				
03 Oct 2000	Urban	46	50	40	86.96	80.00	87.00	0.84
	Forest	49	50	41	83.67	82.00		
	Grassland	65	50	46	70.77	92.00		
	Agriculture	44	50	42	95.45	84.00		
	Water	48	50	45	93.75	90.00		
	Barren land	48	50	47	97.92	94.00		

Note: "Reference totals" means the number of reference pixels that belong to a specific category in the classified image. "Classified totals" shows the number of pixels that were chosen from the entire image to represent specific category in the classified image. "Number correct" shows the number of pixels classified right according to the reference. "Producer's accuracy" is the ratio between number correct and reference totals. "User's accuracy" is the ratio between number correct and classified totals. "Overall accuracy" is the ratio between total number correct and total classified totals. "Overall kappa statistics" indicates the accuracy of classification.

the accuracy of each classified image by the use of stratified random sampling method. The results are listed in Table 3, which shows that the overall accuracy of the classified images was all above 85 percent.

Figure 2 includes an example of classified LULC image acquired on 16 June 2001 with 15 m resolution. These four images were individually resampled to different pixel sizes: 30 × 30 m, 60 × 60 m, 120 × 120 m, 250 × 250 m, 500 × 500 m, and 1,000 × 1,000 m by using the Nearest Neighbor method of resampling. The eight different pixel sizes correspond to the spatial resolutions of different sensors. For example, 15 m resolution corresponds to ASTER visible bands (green and red bands); 30 m resolution corresponds to Landsat TM and ETM+ reflected bands; 90 m corresponds to ASTER TIR bands; 1,000 m resolution responds to AVHRR local coverage bands. Table 4 lists some examples of remote sensing sensors and their spatial resolutions. By examining the LULC and LST at various resolutions, we intended to better understand their interplay at different scales and to find the optimal scale for the study.

LST Derivation

Many algorithms have been developed to retrieve LSTs from different thermal infrared (TIR) sensors. In this study, land surface kinetic temperature data were purchased from NASA with 90 m resolution through a free entry. The temperature-emissivity separation algorithm was applied to compute land surface kinetic temperatures (ASTER products description 2005). According to the product description, the absolute accuracy of the kinetic temperature data is accurate within 1.5°K and relative accuracy 0.3°K. Each LST image was resampled to possess the same pixel sizes as what LULC maps have (i.e., 15 m, 30 m, . . . , 1,000 m) by using the Nearest Neighbor method of resampling. After resampling, each LST map was divided into six temperature zones by the use of the natural break method (Brewer and Oickle, 2002; Smith, 1986). Figure 2 includes a LST map with 90 m resolution on 16 June 2001 as an example. The temperature zone in red was the "hot spot", while the dark blue zone represented the coldest temperature in the area.

Landscape Metrics

Among existing landscape metrics, the average perimeter-area ratio, contagion, standardized patch shape, patch perimeter-area scaling, large-patch density-area scaling, and patch classes were believed to be the most effective indices which could characterize and quantify the spatial characteristics of the landscape pattern (Riitters *et al.*, 1995). In this study, four class-based and six landscape-based metrics were computed for the LULC and LST maps to identify the changes of landscape and LST patterns at different scales at different seasons. Table 5 lists these landscape metrics, their definitions, and formulas. The Patch Percentage Index shows the proportion of each patch type within the landscape; the value is between 0 and 100. It would be 100 when the region only has a single patch class, and it would be close to zero when the corresponding patch class is rare in the region. The Patch Density Index expresses the number of patches per 100 hectares. The value is larger than zero and

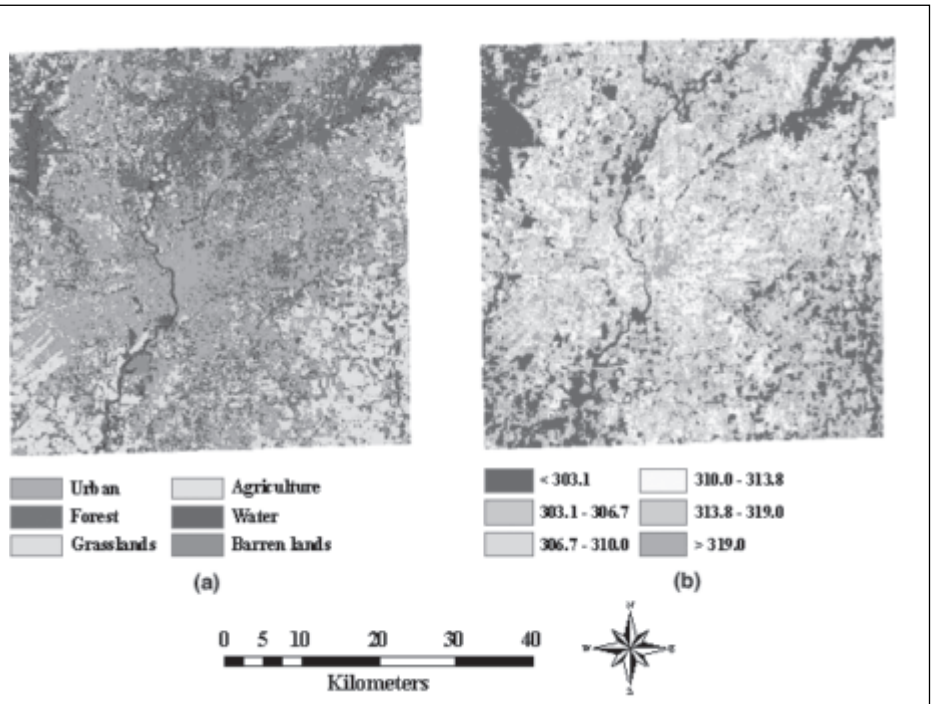

Figure 2. LULC and LST maps for the City of Indianapolis, Indiana on 16 June 2001: (a) LULC map, and (b) LST map with units of °K. A color version of this figure is available at the ASPRS website: **www.asprs.org**.

TABLE 4. EXAMPLES OF REMOTE SENSING IMAGERY

Sensors	Bands	Wavelength ranges (μm)	Resolutions (meter)
ASTER	1–3	0.52–0.86	15
Landsat ETM+	8	0.52–0.90	
ASTER	4–9	1.60–2.43	30
Landsat ETM+	1–5	0.45–1.75	
ALI EO-1	1–9	0.43–2.36	
EO-1 Hyperion	1–242	0.36–2.58	
Landsat ETM+	6	10.40–12.50	60
ASTER	10–14	8.13–11.65	90
Landsat TM	6	10.40–12.50	120
EO-1 LEISA AC	1–309	0.89–1.58	250
MODIS	1–2	0.62–0.88	
MODIS	3–7	0.46–2.16	500
MODIS	8–36	0.41–14.39	1000

reaches the maximum when every cell is a separate patch. The Landscape Shape Index simply measures the class aggregation; the value is more than one and increases as the patch types become more disaggregated. The Perimeter-area Fractal Dimension index quantifies the complexity of the planar shapes, and is identified by means of linear regression and reflects the shape complexity of the patch class. The value is greater than 1 for a two-dimensional landscape when a departure from a Euclidean geometry occurs. It implies more a complicated shape for the patch class when the value is closer to 2. The Mean Perimeter-area Ratio Index simply examines the shape complexity of the landscape; the value is larger than zero without limitation. The Proximity Index examines the proximity of neighboring habitat patches for the focal patch within a specified distance; the value is greater than zero without limitation and increases as the neighborhood is increasingly occupied by patches of the same class. The Cohesion Index measures the physical connection of the corresponding patch type. The Contagion Index examines the aggregation of landscape; the value is close to 1 when the patch types are maximally disaggregated and reaches 100 when the landscape consists of only one patch (McGarigal and Marks, 2002).

The indices were computed for all sixty-four images by the use of FRAGSTAT, a software for quantifying the landscape pattern by the use of landscape metrics (McGarigal *et al.*, 2002). The measurements of four class-based metrics were plotted to reflect the scaling-up effect on the analysis of landscape and LST patterns. Seven landscape-level metrics (Patch Density, Landscape Shape Index, Perimeter-area Fractal Dimension Index, Mean Perimeter-area Ratio, Proximity, Cohesion, and Contagion Index) were used to create multi-dimensional metric spaces for urban areas and the whole study area. Each metric represented one dimension in the space. The shortest distance between LULC and LST maps in the metric space was determined by the calculation of Euclidean distance. All landscape-based indices were standardized to the range from 0 to 1 before it was inputted into the calculation of Euclidean distance since individual index had different unit of measurement.

Results

Scaling-up Effect on Area Percentage

The Patch Percentage Index is the proportion of each patch type within the study area (McGarigal *et al.*, 2002). According to the results, the area percentages of LULC patches in four seasons appeared to be constant across the scales, except that slight variations were observed as the scale changed from 500 m to 1,000 m for urban, forest, and grassland. It indicates that

TABLE 5. DESCRIPTIONS AND EQUATIONS FOR CHOSEN LANDSCAPE METRICS (MCGARIGAL *ET AL.*, 2002)

Metrics	Abbreviations	Definitions	Equations
Percentage of Landscape	PLAND	Proportional abundance of a class	$\text{PLAND} = P_i = (100 * \sum_{j=1}^{n} a_{ij})/A$ P_i: proportion of the landscape occupied by patch type i. a_{ij}: area (m^2) of patch *ij* A: total landscape area (m^2)
Patch Density (class level)	PD	Densities of patches	$\text{PD} = n_i * 10{,}000 * 100/A$ n_i: number of patches in the landscape of patch type i A: total landscape area (m^2)
Landscape Shape Index (class level)	LSI	a measure of class clumpiness	$\text{LSI} = e_i/\min e_i$ e_i: total length of edge of class i in terms of number of cell surface min e_i: minimum total length of edge of class *i* in terms of number of cell surfaces
Perimeter-area Fractal Dimension (class level)	PFRACAC	Shape index based on perimeter and area measurement	$\text{PAFRAC} = \{2/\{[n_i * \sum_{j=1}^{n} (\ln P_{ij} * \ln a_{ij})] - [(\sum_{j=1}^{n} \ln P_{ij})(\sum_{j=1}^{n} \ln a_{ij})]\}\}/[(n_i * \sum_{j=1}^{n} \ln(p_{ij})^2 - (\sum_{j=1}^{n} \ln p_{ij})^2]$ a_{ij}: area (m^2) of patch *ij* p_{ij}: perimeter (m) of patch *ij* n_i: number of patches in the landscape of patch type i
Patch Density (landscape level)	PD	Densities of patches	$\text{PD} = N * 10{,}000 * 100/A$ N: total number of patches in the landscape A: total landscape area (m^2)
Landscape Shape Index (landscape level)	LSI	a measure of class clumpiness	$\text{LSI} = E/\min E$ E: total length of edge in landscape in terms of number of cell surfaces min E: minimum total length of edge in landscape in terms of number of cell surfaces
Perimeter-area Fractal Dimension (landscape level)	PFRACAC	Shape index based on perimeter and area measurement	$\text{PAFRAC} = 2/\{\{[n_i * \sum_{j=1}^{n} (\ln P_{ij} * \ln a_{ij})] - [(\sum_{j=1}^{n} \ln P_{ij})(\sum_{j=1}^{n} \ln a_{ij})]\}\{(N * \sum_{j=1}^{n} \ln(p_{ij})^2 - (\sum_{j=1}^{n} \ln p_{ij})^2\}\}$ a_{ij}: area (m^2) of patch *ij* p_{ij}: perimeter (m) of patch *ij* n_i: total number of patches in the landscape
Mean Perimeter-area Ratio	PARA_MN	Mean value of a shape index	$\text{PARA\_MN} = (\sum_{i=1}^{m} \sum_{j=1}^{n} (p_{ij}/a_{ij}))/N$ a_{ij}: area (m^2) of patch ij p_{ij}: perimeter (m) of patch ij N: total number of patches
Proximity index	PROX	Landscape proximity	$\text{PROX} = \sum_{k=1}^{n} (a_{ijk}/h_{ijk})$ a_{ijk}: area (m^2) of patch ijs within specified neighbourhood (m) of patch ij h_{ijk}: distance (m) between patch ijs and patch ijs based on patch edge-to edge distance
Patch Cohesion index	COHESION	Connectivity index. The physical connectedness of	$\text{COHESION} = [1 - (\sum_{j=1}^{n} P_{ij})/\sum_{j=1}^{n} (P_{ij} * \sqrt{a_{ij}})](1 - 1/\sqrt{A})^{-1} * 100$ P_{ij}: perimeter of patch ij in terms of the patch type number of cell surfaces a_{ij}: area of patch ij in terms of number of cells A: total number of cells in the landscape
Contagion index	CONTAG	Landscape contagion	$\text{CONTAG} = 1 + \frac{\sum_{i=1}^{m} \sum_{k=1}^{m} [P_i * (G_{ik}/\sum_{k=1}^{m} G_{ik})] * (\ln P_i (G_{ik}/\sum_{k=1}^{m} G_{ik}))}{2 \ln m} * 100$ P_i: proportion of the landscape occupied by patch class i g_{ik}: number of adjacencies between pixels of path class i and k based on the double-count method m: number of patch classes present in the landscape

the measurement of patch percentages for individual LULC types was more reliable with image resolutions higher than 500 m. Beyond 500 m resolution, the patch percentage derived from remote sensing data would have much lower accuracy. The shortage of seasonal differences indicates that the measurements of area percentages for all the LULC types are not susceptive to the seasonal changes. Urban tended to increase in area percentage as the scale changed from 500 m to 1,000 m resolution, but forest and grassland possessed a converse tendency simultaneously. As a contrast, water, agriculture, and barren land showed much less sensitivity in the measurement of area percentage. This indicates that the top LULC types in area percentage tended to be more affected by the scaling-up process. It could be explained by a consideration that more forest and grassland patches were aggregated into urban patches in the scaling up process, but much less for water, agriculture, and barren land. This explanation was supported by the phenomena that a great portion of forest and grassland fractionally distributed in the urban area and much less urban patch could be found around aquatic systems, agriculture, and barren land. Although the variations of the measurement were observed, the slight changes implicate that area percentage can be considered as a scale-independent parameter when remote sensing imagery with corresponding resolutions are applied in urban planning and environmental management, such as LULC monitoring and habitat conservation.

LST patches in the four dates possessed more variations in area percentage across the seasons and spatial scales compared to those of LULC patches. On 06 February 2006, Zones 1, 2, 3, and 4 showed up and down variations across the scales. Zone 1 and 4 even intersected in several scales since their percentages were so close. Zone 5 and 6 appeared to be constant across the resolutions as temperature zones with the least area percentages. It indicates that the top temperature zones in area percentage showed more obvious variations across the scales since more pixels in the top zones were re-assigned new values during the scaling-up process and was classified to different classes based on the algorithm of natural break classification.

On 05 April 2004, the area percentages of all zones remained constant across the scales until the resolution reached 250 m. Starting from 250 m, the top zone, Zone 3, showed a slight decrease in area percentage, and Zones 2 and 4 separated from each other and showed opposite variations, as do Zones 1 and 5. Zone 6 (the zone with the highest temperature) experienced slightly increase at the same time. It implies that the zones with median area percentages in the study area tended to be easier to be impacted during the scaling-up process. As a contrast, the zones with the highest and lowest area percentages possessed much less impact.

On 16 June 2001, Zones 2 and 3 met in several places since their area percentages were very close. Zones 1 and 4 intersected in 250 m resolution which indicates that the area percentages for both zones tended to be susceptive to the aggregation process at specific resolution. The area percentage of Zone 1 tended to decrease starting from the scale of 120 m, and Zones 2, 3, and 4 experienced decreases starting from 250 m resolution. Both Zones 5 and 6 possessed little variations in area percentage across the scales until the scale reaches 250 m.

On 03 October 2000, the top zone in area percentage (Zone 3) did not show significant variations across the scales. Zones 2 and 4 were the second top zones in area percentage, and their percentages showed much more obvious changes across the scales, but they did not meet each other at any scale. Zones 1 and 5 intersected between 250 m and 500 m resolution, which indicates that the zones with the lowest temperature and the second highest temperature tended to be susceptive to the aggregation process when the resolution changes between 250 m and 500 m. Zone 6 did not seem to be significantly affected by the scaling process. The area percentages of LULC and LST patches across eight scales on 16 June 2001 were plotted in Figure 3 as an example.

Scaling-up Effect on Patch Density

The Patch Density Index indicates the number of patches per 100 hectares (McGarigal *et al.*, 2002). According to the result, the patch densities of LULC types kept decreasing with the decrease of spatial resolutions without seasonal difference. The measurement of patch densities for individual LULC

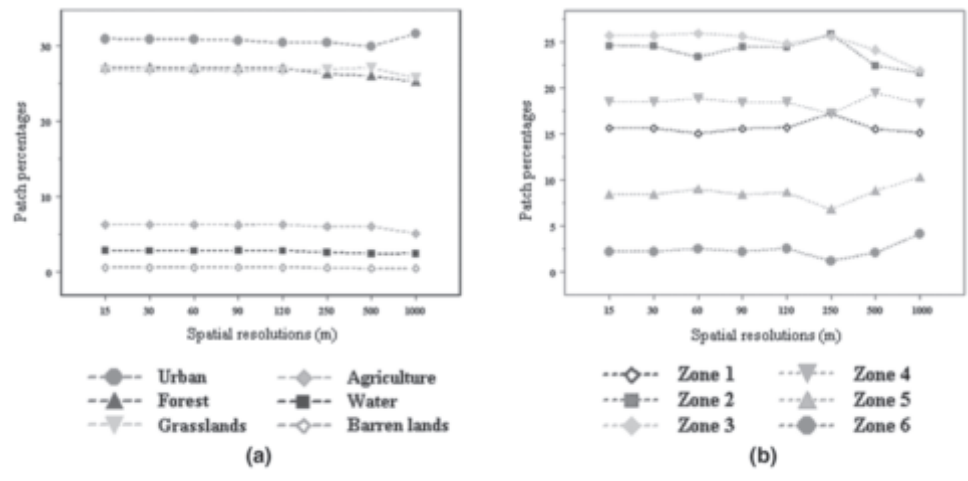

Figure 3. Patch percentages derived from sample LULC and LST maps (using image date 16 June 2001 as an example); *x*-axis shows the scales, and *y*-axis shows the values of the metric: (a) LULC map, and (b) LST map. A color version of this figure is available at the ASPRS website: **www.asprs.org**.

types became less reliable when the resolution was lower than 120 m in the study area since the patch densities of all LULC categories tended to be equal after 120 m resolution. In each season, the slopes of decrease were quite sharp for urban, forest, and grassland before the scale reached 60 m, and then became gentler toward 1,000 m resolution. The overall decreases were much gentler for water, agriculture, and barren land across the scales. It indicates that the top LULC types in density appeared to be easily susceptive to the scaling-up process, but not for the LULC types with relatively low patch densities for each season. It could be explained by the fact that the patch numbers of urban, forest, and grassland significantly declined during the aggregation process in the study area. The variations of patch densities for LULC and LST maps across eight scales in 16 June 2001 are shown in the Figure 4.

LST patch densities showed similar tendencies of change across the seasons and scales, although these seasons had different top zones in patch density. The calculation of patch densities for individual LST zones was not acceptable when the resolution was lower than 120 m in the study area since the patch densities of some LST zones (e.g., Zone 1 and Zone 5) tended to be equal at 250 m resolution. All patch densities of temperature zones tended to be equal at 1,000 m resolution, which indicates a maximum patch aggregation at the scale of 1,000 m. It indicates that sensors with 1,000 m resolution might not be a good choice when urban planners and environmental management agencies are focused on the study of LST patch density and related issues.

On each date, patch densities did not possess obvious variations as the scale changed from 15 m to 90 m, but sharp decreases were observed as the scale changed from 90 m to 1,000 m (Figure 4). The effect was more obvious for LST zones with high densities (Zones 3 and 4 on 06 February 2006, Zones 2, 3, and 4 on 05 April 2004, Zones 3 and 4 on 16 June 2001, and Zones 3 and 4 on 03 October 2003). They demonstrated sharper slopes of declines starting from 90 m resolution and indicate prominent impacts caused by the scaling-up process. It was clear that the higher the patch density, the more variations the temperature zone possessed across the scales. Zone 6 possessed the least variations across the scales in each season due to its lowest value in patch density.

Scaling-up Effect on Landscape Aggregation

The Landscape Shape Index simply measures the aggregation of landscape, and its value increases as the patch type becomes more disaggregated (McGarigal *et al.*, 2002). The measurement of index for LULC and LST patches were plotted in Figures 5 with an image date 16 June 2001 as an example. The calculation of patch aggregation for individual LULC types became less acceptable when the resolution was lower than 120 m since the values of Landscape Shape Index for water and agriculture tended to be equal after 120 m resolution. No distinct seasonal changes could be observed in the Figure 5 except that grass land was the top LULC type in Landscape Shape Index in all dates but not on 06 February 2006. Similar to Patch Density, Landscape Shape indices derived from LULC maps showed constant decreases across the scales in each season, especially for urban, forest, and grassland (Figure 5). They experienced great declines compared to the rest three LULC types, agriculture, water, and barren land. It indicates that relatively highly disaggregated LULC types would experience much more change in the aggregation process across the scales compared to the ones with better aggregation level from the beginning. It could be explained by the urbanization in the study area; urban construction, grassland, pasture, and urban forest were mixed together and greatly impacted each other's aggregation level. Agriculture, water, and barren land possessed much fewer variations since they were minor LULC types in area percentage in the study area and away from the process of urbanization. In Figure 5, grass showed a relatively high aggregation measurement in year 2000 and 2001 images, but the values dropped in the 2004 and 2006 images. It indicates that urbanization had significant impact on the aggregation of grassland. The overall decline of the measurements for LULC types was not counterintuitive for the metric, since the aggregation level of the whole landscape would increase as the spatial resolution becomes coarser. The rates of decline appeared to be constant across the scales without any observation of critical scale(s).

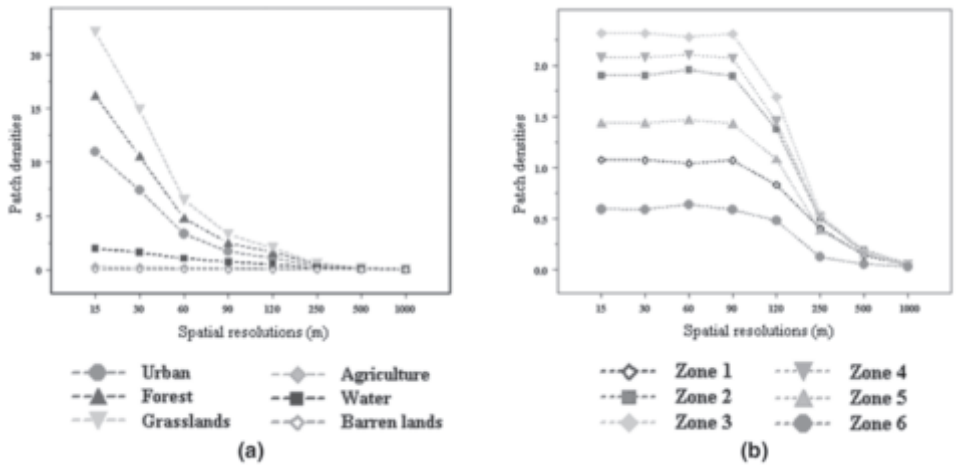

Figure 4. Patch densities derived from LULC and LST maps (using image date 16 June 2001 as an example); *x*-axis shows the scales, and *y*-axis shows the values of the metric: (a) LULC map, and (b) LST map. A color version of this figure is available at the ASPRS website: **www.asprs.org**.

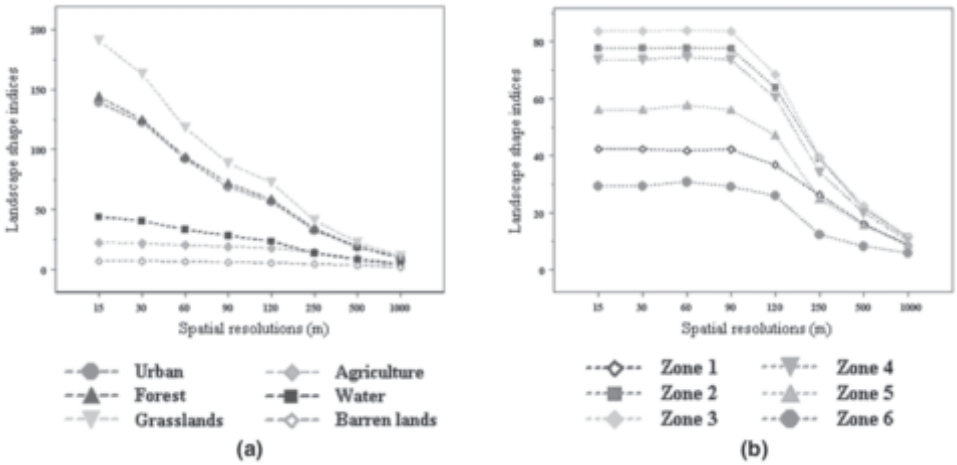

Figure 5. Landscape Shape Indices derived from LULC and LST maps (using image date 16 June 2001 as an example); *x*-axis shows the scales, and *y*-axis shows the values of the metric: (a) LULC map, and (b) LST map. A color version of this figure is available at the ASPRS website: **www.asprs.org**.

The measurements of the Landscape Shape Index for all temperature zones showed similar variations across the scales and seasons (Figure 5). The measurement of patch aggregation for individual LST zones became less and less reliable when the resolution was lower than 120 m in the study area since the measurement of the Landscape Shape Index for some LST zones tended to be equal after 120 m resolution and aggregation of all the zones tended to be equal at 1,000 m resolution. The indices did not have obvious changes until the scale reached 90 m for each date, and then kept decreasing until 1,000 m. These declines seemed to be especially obvious for Zones 2, 3, and 4 for each date, but not for Zone 1, 5, and 6. It indicates that the zones with relatively higher values of index were maximally affected by the scaling-up process compared to any other zones. The index showed predictable results across the scales, since the measurement of index was expected to decrease when the landscape became more aggregated.

Scaling-up Effect on Fractal Dimension

The Perimeter-area Fractal Dimension Index reflects the shape complexity of patch, class or the whole landscape (McGarigal *et al.*, 2002). The primary significance of shape in determining the nature of patches is related to edge effect, an important topic closely related to various spatial patterns. For example, forest edge effect can influence vegetation composition and structure (McGarigal *et al.*, 2002; Ranney *et al.*, 1981). The Perimeter-area Fractal Dimension Index was developed based on an idea of statistical self-similarity and a fundamental hypothesis that there is a power law relationship between area and perimeter of patches, classes, and the whole landscape; the pattern of self-similarity may change and the hypothesis may be violated during the aggregation process since the development of perimeter area regression may experience unexpected change during the process, such as goodness of fit and the calculation of *y*-intercept (Frohn 1998). The index is believed to be sensitive to the number of patches, the range of patch sizes, and the mixing of LULC types. The results can be unpredictable when the spatial resolutions vary due to the changes of *y*-intercept.

As a result, the measurements of the Perimeter- area Fractal Dimension Index obtained unexpected results for both LULC and LST maps without significant seasonal differences (see image dated 16 June 2001 in Figure 6 for an example). The overall increase of fractal dimension for each season was counterintuitive for the metric because the fractal dimension was expected to decrease with the decrease of aggregation from 15 m to 1,000 m. The discovery was consistent with the results reported by Frohn, which showed that the scaling-up processes could affect linear regress, the base of the formula to calculate the fractal dimension (Frohn 1998). Seasonal changes did not show significant impact on the measurement of the index across the scales.

The Perimeter- area Fractal Dimension Indices derived from LST maps showed unexpected but more complicated variations than those derived from LULC maps. Seasonal differences could not be observed for the measurements of the index across the scales. The measurement of fractal dimension for each temperature zone for every season did not show significant changes as the scale changed from 15 m to 30 m resolution and then experienced a nadir at 60 m resolution. It indicates that the *y*-intercept in the regressing analysis experiences a significant change at 60 m resolution for each zone. The values of the calculations kept increasing as the scale changed from 60 m to 250 m for each date and showed diverse variations after 250 m resolution.

Modified Fractal Dimension Indices could be used to improve the result (Frohn, 1998). Frohn developed an improved equation to identify the shape complexity of landscape patterns, which was believed to be more predictable across the scales, since it did not rely on the assumption of a power law relationship between area and perimeter. The formula is given below:

$$S = 1 - 4^{*}A^{1/2}/P \quad (1)$$

where S is Improved Fractal Dimension Index, A is the total area of all patches, and P is the total perimeter of all patches in the study area.

In order to examine its capability in the examination of shape complexity, the modified Fractal Dimension was

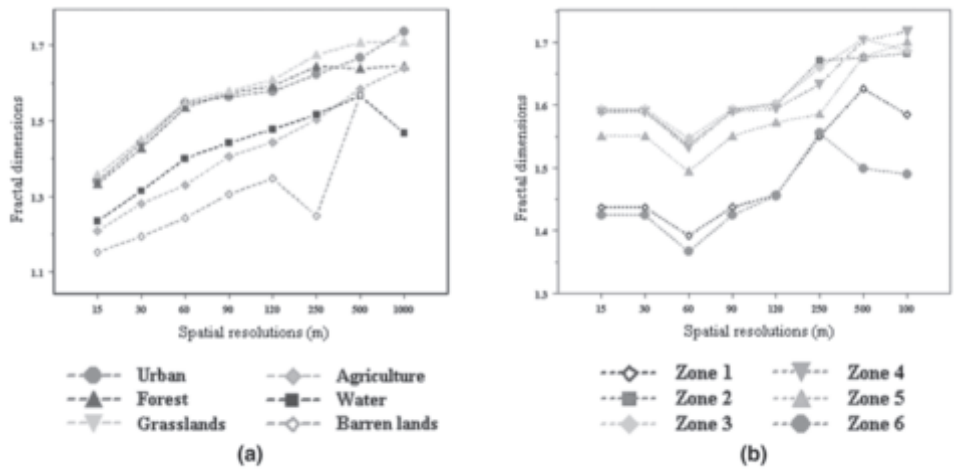

Figure 6. Patch Fractal Dimensions derived from four LULC maps; *x*-axis shows the scales, and *y*-axis shows the values of the metric: (a) LULC map, and (b) LST map. A color version of this figure is available at the ASPRS website: **www.asprs.org**.

computed for the LST maps in each date. The information of fractal dimension for individual LST categories started to be lost when the resolution kept decreasing from 120 m to 1,000 m. In each season, the values of improved fractal dimensions did not show clear changes as the scale changed from 15 m to 120 m resolution, and starting from 120 m resolution, the values kept declining to the end with increasing slopes of change. Zones 1, 5, and 6 possessed much more variation in the measurement of improved metric across the scales than those of Zones 2, 3, and 4. The variations among different zones indicate that temperature zones with lower shape complexity were more sensitively affected in the measurement of the improved metric during the scaling-up process. It is noted that Zones 1, 5, and 6 were the zones with the lowest and highest temperatures and showed relatively low area percentages, patch densities, and aggregation levels across the scales. They were greatly dispersed by any other temperature zone in the study area, and their complexity became extremely simple since many of their pixels might be classified to any other temperature zones during the aggregation process. The measurements for image date 16 June 2001 are shown in Figure 7.

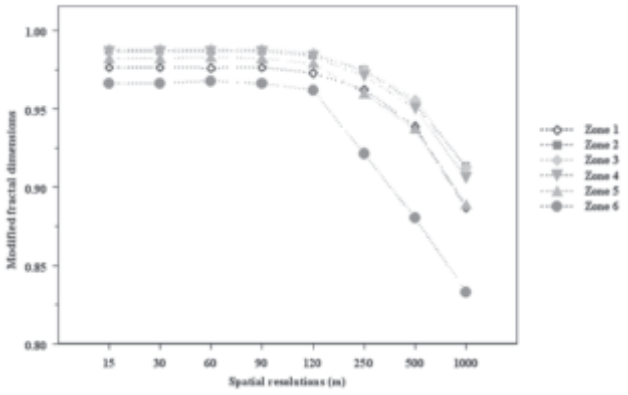

Figure 7. Modified fractal dimensions for LST map (using image date 16 June 2001 as an example). A color version of this figure is available at the ASPRS website: **www.asprs.org**.

Spatial Agreement between Landscape and LST Patterns

According to the results analyzed above, multiple resolutions were observed as critical scales for the identification of LULC and LST patterns by the use of various landscape metrics. However, no optimal resolution was pointed out to examine the relationships between landscape and LST patterns. In this paper, a method was developed to identify the optimal spatial scales for one of the LULC categories, urban area in the study area and for the whole study area itself. Urban landscape patterns and its LST were separated from the whole study area in each four image dates. Four urban LST maps were individually classified to have six classes by the Natural Break method. Four urban landscape maps and four classified urban LST maps were resampled to have the scales of 15 m, 30 m, 60 m, 90 m, 120 m, 250 m, 500 m, and 1,000 m. Six landscape-level metrics, Patch Density, Perimeter- area Fractal Dimension Index, Mean Perimeter-area Ratio, Proximity, Cohesion, and Contagion Indices formed a six-dimension metric space for the urban areas.

Normalized Euclidean Distances between urban landscape and LST maps for each image date are shown in Figure 8, which shows that the values of Normalized Euclidean Distance reached a minimum at 30 m resolution for all seasons. It implies that the spatial structures of both LST and urban landscape patterns, as identified by the class-based landscape metrics, tended to be most comparable as the scale reached 30 m resolution. As a result, 30 m resolution was believed to be the optimal spatial scale to examine the class-based relationship between LSTs and landscape patterns for the study area.

As for the whole study area, six landscape-level metrics, Patch Density, Landscape Shape Index, Perimeter- area Fractal Dimension Index, Mean Perimeter-area Ratio, Proximity, and Contagion Index were chosen to create the multi-dimension landscape metric space. The Normalized Euclidean Distances between each pair of LULC and LST maps with the same spatial resolution were calculated and standardized in the metric space for the whole study area (Figure 9). The result showed that the Normalized Euclidean Distance for

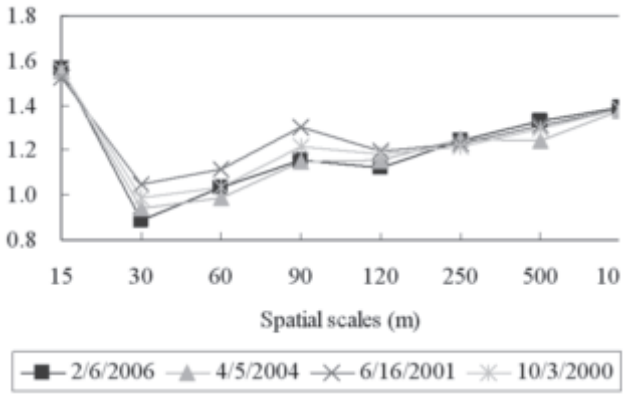

Figure 8. Eculidean distances between two points in the landscape metrics space for Urban landscape and LST maps with the same spatial resolution. A color version of this figure is available at the ASPRS website: **www.asprs.org**.

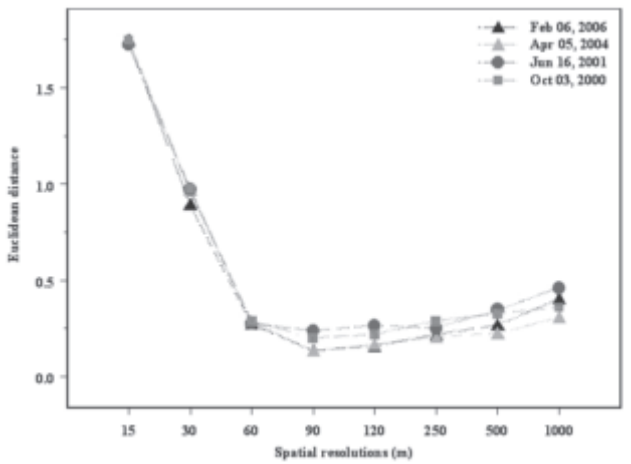

Figure 9. Eculidean distances between two points in the landscape metrics space for LULC and LST maps with the same spatial resolution. A color version of this figure is available at the ASPRS website: **www.asprs.org**.

each season kept declining from 15 m to 60 m resolution with a very high slope and reached the minimum at 90 m resolution with a much gentle slope. It implies that the spatial structures of both LST and LULC patterns identified by the landscape metrics possessed significant variations and tended to be more comparable as the scale changed from 15 m to 90 m resolution. Figure 9 shows that the Normalized Euclidean Distance Line started to rise from 90 m to 1,000 m with a much gentler slope. It indicates that the 90 m resolution should be the optimal spatial scale to examine the landscape-level relationship between LSTs and landscape patterns since the Normalized Euclidean Distance reached the minimum for all dates, and the spatial characteristics of LULC and LST patterns were at the most comparable status at this resolution

In order to further examine how the Normalized Euclidean Distance changed with spatial resolution, the LULC and LST images were re-sampled at the spatial resolutions of 20 m, 40 m, 50 m, 70 m, 80 m, 100 m, 200 m, 300 m, 400 m, 600 m, and 800 m, in addition to the seven resolution levels discussed above. A data fitting was then performed based on the Normalized Euclidean Distances at these nineteen different scales. Figure 10 shows a three-dimensional observation of the Normalized Euclidean Distances across the scales and seasons. Figure 11 plots the regression lines as a result of data fitting. Equation 2 is the nonlinear regression model for the fitting:

$$Y = \begin{cases} 13.2545^{*}X^{\wedge}(-0.6294) - 0.6739 (15 <= X <= 90) \\ 0.00771^{*}\mathrm{e}0.00299^{*}X + 0.21152 (90 < \mathrm{X} <= 1000) \end{cases} \quad (2)$$

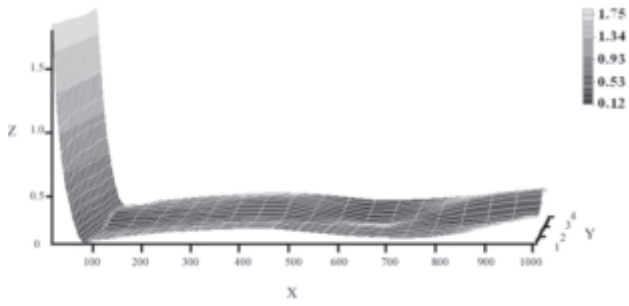

Figure 10. 3D visualization of the Normalized Euclidean Distances (*Z*-axis) across the scales (*X*-axis) and seasons (*Y*-axis). In *Y* axis, 1, 2, 3, and 4 individually represents the date 16 February 2006, 05 April 2004, 16 June 2001, and 03 October 2000. Light (blue) color corresponds to higher Euclidean distances and dark (blue) colorss correspond to lower values. Significant decreases were observed when the spatial scales decreased from 15 m to 90 m. A color version of this figure is available at the ASPRS website: **www.asprs.org**.

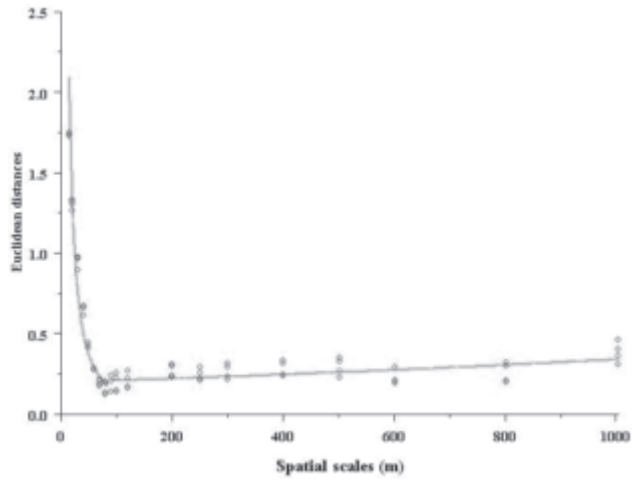

Figure 11. Nonlinear regressing line between the spatial scales and Euclidean distances. Light (green) line is the regression line and dark (red) spots are samples. A minimum value was observed at 90 m spatial resolution. A color version of this figure is available at the ASPRS website: **www.asprs.org**.

where Y is the Normalized Euclidean Distance, and X is the spatial resolution. From this equation, it is noted that the first portion of the equation had a much steeper slope than that of the second portion, suggesting that the spatial agreement between landscape patterns and LSTs rapidly increased as the spatial resolution changed from 15 m to 90 m. After 90 m, the slope became much gentler, implying that the spatial agreement tended to decrease at a slow rate.

Discussion and Conclusions

This research has examined the scaling-up effect on the relationship between landscape patterns and LSTs for Indianapolis in four seasons with an integration of remote sensing, GIS, and a landscape ecology approach. The following conclusions may be summarized:

- Patch Percentage expresses the proportion of each patch type within the landscape. In this study, we found that three LULC types, namely, urban, forest, and grassland, were more sensitively affected by the aggregation process compared to three other LULC types, i.e., water, agriculture, and barren land. LST patches showed more noticeable variations (as compared to LULC patches) in the area percentage index across the scales without significant seasonal differences. For this metric, no scale threshold could be identified to show serious degradation with decreasing resolution.
- Patch Density expresses the number of patches per 100 hectares. We found that the slope of decrease was sharper for urban, forest, and grassland than that for water, agriculture, and barren land across the scales. Zones close to the median LST values, namely, Zones 2, 3, and 4, were maximally affected by the scaling-up process. For this metric, scales above the threshold 120 m began to show serious degradation with increasing scale.
- The Landscape Shape Index measures the class aggregation. The values of the Landscape Shape Index for both LULC and LST maps kept decreasing across the scales in all seasons. For this metric, scales above the threshold 120 m began to show serious degradation with decreasing resolution.
- The Improved Fractal Dimension Index was employed to quantify the shape complexity of the temperature zones. We found that three temperature zones with the minimum and maximum temperature values, namely, Zones 1, 5, and 6, possessed more noticeable variations across the scales than those of Zones 2, 3, and 4. For this metric, scales above the threshold 120 m began to show serious degradation with increasing scale.
- Overall, our conclusion is that landscape metrics, including, Patch Density, Landscape Shape Index, and Improved Fractal Dimension could be employed to effectively quantify the spatial patterns and changes of LULC types and temperature zones.
- The threshold of 90 m was suggested to be the optimal spatial resolution to examine the relationship between landscape patterns and LSTs for the whole city (at the landscape-level), while 30 m resolution was believed to be the optimal spatial scale to examine the *class-based* relationship between LST and LULC for the study area. This finding could contribute to the sensor selection and mapping of urban landscapes, as well as natural resource management by the use of remote sensing data.

Using remote sensing techniques to assess the scaling effects on the relationship between landscape pattern and land surface temperature is still a challenging task due to the quality of remote sensing data, acquisition time, processing methods, and the accuracy and sensitivity of individual landscape metrics. This study demonstrates that ASTER imagery may be used to examine the scaling effect. Results indicate that the scaling-down method chosen in the study did not apparently affect measurement of patch density and aggregation when LST resolutions were 15 m, 30 m, and 60 m. The patch numbers and aggregation levels of LST at these resolutions remained the same as those in the 90 m resolution LST map. The differences between LULC and LST patterns were due mainly to the resampling method used, i.e., the Nearest Neighbor method. This method uses the value of the closest pixel in the input image to assign to the output pixel value (Avery and Berlin, 1992).

In order to examine whether the measurements of Patch Density and Landscape Shape Indices were sensitive to resampling methods, the Bilinear Interpolation method was applied to compare with the Nearest Neighbor method. The image of 16 June 2001 was chosen for the test. The results showed that the measurements of both Patch Density and Landscape Shape Indices for LULC types kept decreasing across the scales, just like the patterns of changes reflected in Figure 4 and Figure 5. But, for the LST map, the measurements of the two metrics showed different results (Figure 12). For the measurement of Patch Density, the difference was that the patch densities of temperature zones with median temperatures, namely, Zones 2, 3, and 4, increased when the scale changed from 60 m to 90 m. This result contradicted the fact that the patch density should decrease when the scale became coarser. The contradiction implies that the Patch Density metric was much more sensitive to the Bilinear Interpolation method than the Nearest Neighbor method.

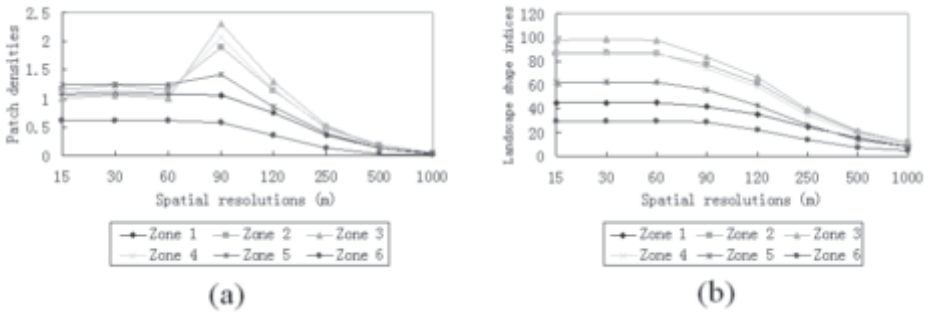

Figure 12. The measurements of Patch Density and Landscape Shape Index for LST map in image dated 16 June 2001 by using Bilinear Interpolation method to resample images: (a) shows the measurements of patch densities, and (b) shows the measurements of landscape shape indices. A color version of this figure is available at the ASPRS website: **www.asprs.org**.

For the Landscape Shape Index, the difference was that the value of the index started to significantly decrease when the scale reached 60 m resolution, instead of 90 m resolution in the Figure 5. However, with either the Nearest Neighbor method or the Bilinear Interpolation method, 120 m was shown to be a critical resolution in the study of scaling effects by using the Landscape Shape Index.

The measurement of Perimeter-area Fractal Dimension showed that for both LULC and LST maps in each season, its value kept increasing with the decreases of resolution. This increase is in contradiction with the conventional concept that fractal dimension decreased with more aggregated landscapes. The sensitivity of the formula used to calculate fractal dimension was believed to cause this contradiction. As a result, more caution needs to be taken when this metric is used in the aggregation process, and any conclusion should not be made without a detailed examination of the possible effect to the computation of metric. Furthermore, although the results from the Improved Fractal Dimension Index (with Equation 2) did not contravene the conventional concept, this method has not been validated. It is necessary to document how the improved metric performs for study areas with mixed LULC types. Since fractal dimension is an important metric to quantify the shape of landscape patterns, the landscape-level fractal dimension metric (Table 5) was still used as one of the dimensions in the metric space to identify the optimal spatial scale for the urban areas and the whole study area.

Acknowledgments

This research was supported by National Science Foundation (BCS-0521734) for a project entitled "Role of Urban Canopy Composition and Structure in Determining Heat Islands: A Synthesis of Remote Sensing and Landscape Ecology Approach." We would also like to thank three anonymous reviewers for their constructive comments and suggestions.

References

Agam, N., W.P. Kustas, M.C. Anderson, F. Li, and C.M.U. Neale, 2007. A vegetation index based technique for spatial sharpening of thermal imagery, *Remote Sensing of Environment*, 107(4):545–558.

Aguiar, R., M. Oliveira, and H. Goncalves, 2002. Climate change impacts on the thermal performance of Portuguese buildings: Results of the SIAM study, *Building Service Engineers Research and Technology*, 23(4):223–231.

Allen, T.F.H, R.V. O'Neill, T.W. Hoekstra, 1984. *Interlevel Relations in Ecological Research and Management: Some Working Principles from Hierarchy Theory*, USDA Forest Service General Technical Report RM-110, Fort Collins, Colorado, 11 p.

Aplin, P., 2006. On scales and dynamics in observing the environment, *International Journal of Remote Sensing*, 27(11):2123–2140.

Aplin, P., and P.M. Atkinson, 2004. Predicting missing field boundaries to increase per-field classification accuracy, *Photogrammetric Engineering & Remote Sensing*, 70(1):141–149.

Asner, G.P., M.M.C. Bustamante, and A.R. Townsend, 2003. Scale dependence of biophysical structure in deforested areas bordering the Tapajos National Forest, Central Amazon, *Remote Sensing of Environment*, 87(4):507–520.

ASTER Online Product Description, 2005. NASA web source, URL: *http://asterweb.jpl.nasa.gov/content/03_data/01_Data_Products/SurfaceTemperature.pdf*, National Aeronautics and Space Administration, Washington, D.C. (last date accessed: 16 December 2008).

Avery, T.E., and G.L. Berlin, 1992. *Fundamentals of Remote Sensing and Airphoto Interpretation*, Prentice Hall, Upper Saddle River, New Jersey, 472 p.

Bain, D.J., and G.S. Brush, 2004. Placing the pieces: Reconstructing the original property mosaic in a warrant and patent watershed, *Landscape Ecology*, 19(8):843–856.

Becker, F., and Z.L. Li, 1990. Toward a local split window method over land surface, *International Journal of Remote Sensing*, 11(3):369–393.

Bender, O., H.H., Boehmer, D. Jens, and K.P. Schumacher, 2005. Analysis of land-use change in a sector of Upper Franconia (Bavaria, Germany) since 1850 using land register records, *Landscape Ecology*, 20(2):149–163.

Boyd, D.S., G.M. Foody, P.J. Curran, R.M. Lucas, and M. Honzak, 1996. An assessment of radiance in Landsat TM middle and thermal infrared wavebands for the detection of tropical forest regeneration, *International Journal of Remote Sensing*, 17(2):249–261.

Brewer, C.A., and L. Pickle, 2002. Evaluation of methods for classifying epidemiological data on choropleth maps in series, *Annals of the Association of American Geographers*, 92(4):662–681.

Canway, T.G., 1997. Improved remote heat sensing, *Mechanical Engineering*, 119:88–89.

Chen, D., D.A. Stow, and P. Gong, 2004. Examining the effect of spatial resolution and texture window size on classification accuracy: an urban environment case, *International Journal of Remote Sensing*, 25(11):2177–2192.

Curran, P.J., and P.M. Atkinson, 1998. Geostatistic and remote sensing, *Progress in Physical Geography*, 22(1):61–78.

Franklin, J.F., and R.T.T. Forman, 1987. Creating landscape patterns by forest cutting: Ecological consequences and principles, *Landscape Ecology*, 1(2):5–18.

Frohn, R.C., 1998. *Remote Sensing for Landscape Ecology: New Metric Indicators for Monitoring, Modelling, and Assessment of Ecosystems*, Lewis Publishers, Boca Raton, Florida, 112 p.

Gillespie, A.R., S. Rokugawa, T. Matsunaga, J.S. Cothern, S. Hook, and A.B. Kahle, 1998. A temperature and emissivity and reflection radiometer (ASTER) images, *IEEE Transactions on Geoscience and Remote Sensing*, 36(4):1113–1126.

Gustafson, E.J., 1998. Quantifying landscape spatial pattern: What is the state of the art?, *Ecosystems*, 1(2):143–156.

Hall, F.G., D.E. Strebel, and P.J. Sellers, 1988. Linking knowledge among spatial and temporal scales: Vegetation, atmosphere, climate and remote sensing, *Landscape Ecology*, 2(1):3–22.

Hsieh, P.F., L.C. Lee, and N.Y. Chen, 2001. Effect of spatial resolution on classification errors of pure and mixed pixels in remote sensing, *IEEE Transactions on Geoscience and Remote Sensing*, 39(12):2657–2663.

Huang C., E.L. Geiger, and J.A. Kupfer, 2006. Sensitivity of landscape metrics to classification scheme, *International Journal of Remote Sensing*, 27(14):2927–2948.

Jacob, F., A. Olioso, X. Gu, Z. Su, and B. Seguin, 2002. Mapping surface fluxes using visible, near infrared, thermal infrared remote sensing data with a spatialized surface energy balance model, *Agronomie: Agriculture and Environment*, 22(6):669–680.

Ju, J.C., S. Gopal, and E.D. Kolaczyk, 2005. On the choice of spatial and categorical scale in remote sensing land-cover classification, *Remote Sensing of Environment*, 96(1):62–77.

Kato, S., and Y. Yamaguchi, 2006. Analysis of urban heat-island effect using ASTER and ETM+ data: separation of anthropogenic heat discharge and natural heat radiation from sensible heat flux, *Remote Sensing of Environment*, 99(1–2):44–54.

KrÖnert, R., U. Steinhardt, and M. Volk, 2001. *Landscape Balance and Landscape Assessment*, Springer Verlag, Berlin Heidelberg, New York, 304 p.

Krummel, J.R., R.H. Gardner, G. Sugihara, R.V. O'Neill, and P.R. Coleman, 1987. Landscape patterns in a disturbed environment, *Oikos*, 48(3):321–324.

Li, H., and J. Wu, 2004. Use and misuse of landscape indices, *Landscape Ecology*, 19(4):389–399.

Luvall, J.C., and H.R. Holbo, 1991. Thermal remote sensing methods in landscape ecology, *Quantitative Methods in Landscape Ecology* (M.G. Turner and R.H. Gardner, editors), Springer-Verlag, Berlin Heidelberg, New York, pp. 127–152.

Mandelbrot, B.B., 1983. *The Fractal Geometry of Nature*, W.H. Freeman, San Francisco, California, 480 p.

McGarigal, K., and B.J. Marks, 1995. *FRAGSTATS: Spatial Pattern Analysis Program for Quantifying Landscape Structure*, General Technical Report PNW-GTR-351, USDA Forest Service, Pacific Northwest Research Station, Portland, Oregon, 122 p.

McGarigal, K., S.A. Cushman, M.C. Neel, and E. Ene, 2002. FRAGSTATS: Spatial pattern analysis program for categorical maps. Computer software program produced by the authors at the University of Massachusetts Amherst, URL: *http://www.umass.edu/landeco/research/fragstats/fragstats.html*, University of Massachusetts Amherst, Amherst, Massachusetts (last date accessed: 16 December 2008).

McVicar, T.R., and D.L.B. Jupp, 1998. The current and potential operational uses of remote sensing to aid decisions on drought exceptional circumstances in Australia: A review, *Agriculture Systems*, 57(3):399–468.

Meentemeyer, V., 1989. Geographical perspectives of space, time, and scale, *Landscape Ecology*, 3(4):163–173.

Moody, A., and C.E. Woodcock, 1995. The influence of scale and the spatial characteristics of landscapes on land-cover mapping using remote sensing, *Landscape Ecology*, 10(6):363–379.

Pan, D., G. Domon, D. Marceau, and A. Bouchard, 2001, Spatial pattern of coniferous and deciduous forest patches in an eastern North America agricultural landscape: The influence of land-use and physical attributes, *Landscape Ecology*, 16(2):99–110.

Petit, C.C., and E.F. Lambin, 2001, Integration of multi-source remote sensing data for land-cover change detection, *International Journal of Geographical Information Science*, 15(8):785–803.

Pickett, S.T.A., J. Kolasa, and C.G. Jones, 1994. *Ecological Understanding (The Nature of Theory and the Theory of Nature)*, Academic Press, San Diego, California, 206 p.

Price, J.C., 1983. Estimating surface temperature from satellite thermal infrared data - A simple formulation for the atmospheric effect, *Remote Sensing of Environment*, 13(4):353–361.

Quattrochi, D.A., and M.K. Ridd, 1998. Analysis of vegetation within a semi-arid urban environment using high spatial resolution airborne thermal infrared remote sensing data, *Atmosphere Environment*, 32(1):19–33.

Quattrochi, D.A., and J.C. Luvall, 1999. Thermal infrared remote sensing for analysis of landscape ecological process: Methods and applications, *Landscape Ecology*, 14(6):577–598.

Ranney, J.W., M.C. Bruner, and J.B. Levenson, 1981. The importance of edge in the structure and dynamics of forest islands, *Forest Island Dynamics in Man-Dominated Landscapes* (R.L. Burgess and D.M. Sharpe, editors.), Springer-Verlag, Berlin Heidelberg, New York, pp. 67–94.

Riitters K.H., R.V. O'Neill, C.T. Hunsaker, J.D. Wickham, D.H. Yankee, and S.P. Timmins, 1995. A factor analysis of landscape pattern and structure metrics, *Landscape Ecology*, 10(1):23–39.

Smith, R.M., 1986. Comparing traditional methods for selecting class intervals on choropleth maps, *Professional Geographer*, 38(1):62–67.

Stefanov, W.L., and M. Netzband, 2005. Assessment of ASTER land-cover and MODIS NDVI data at multiple scales for ecological characterization of an arid urban center, *Remote sensing of Environment*, 99(1–2):31–43.

Streutker, D., 2002. A remote-sensing study of the urban heat island of Houston, Texas, *International Journal of Remote Sensing*, 23(13):2595–2608.

Streutker, D., 2003. Satellite-measured growth of the urban heat island of Houston, Texas, *Remote Sensing of Environment*, 85(3):282–289.

Turner, M.G., 1990. Spatial and temporal analysis of landscape patterns, *Landscape Ecology*, 4(1):21–30.

Voogt, J.A., and T.R. Oke, 1997. Complete urban surface temperatures, *Journal of Applied Meteorology*, 36(9):1117–1132.

Voogt, J.A., and T.R. Oke, 2003. Thermal remote sensing of urban climates, *Remote Sensing of Environment*, 86(3):370–384.

Wan, Z., and J. Dozier, 1996. A generalized split-window algorithm for retrieving land-surface temperature from space, *IEEE Transactions on Geoscience and Remote Sensing*, 34(2):892–905.

Wan, Z., and Z.L. Li, 1997. A physics-based algorithm for retrieving land-surface emissivity and temperature from EOS/MODIS data, *IEEE Transactions on Geoscience and Remote Sensing*, 35(4):980–996.

Wan Z., P. Wang, and X. Li, 2004. Using MODIS land surface temperature and normalized difference vegetation index products for monitoring drought in the southern Great Plains, USA, *International Journal of Remote Sensing*, 25(1):61–72.

Wang, Y., X. Zhang, H. Liu, and H.K. Ruthie, 1999. Landscape characterization of metropolitan Chicago region by Landsat TM, *Proceedings of the ASPRS 1999 Annual Conference*, 17–21 May, Portland, Oregon (American Society for Photogrammetry and Remote Sensing, Bethesda, Maryland), pp. 238–247.

Weng, Q., D. Lu, and J. Schubring, 2004. Estimation of land surface temperature-vegetation abundance relationship for urban heat island studies, *Remote Sensing of Environment*, 89(4):467–483.

Weng, Q., D. Lu, and B. Liang, 2006. Urban surface biophysical descriptors and land surface temperature variations, *Photogrammetric Engineering & Remote Sensing*, 72(11):1275–1286.

Wu, J., and R. Hobbs, 2002. Key issues and research priorities in landscape ecology: An idiosyncratic synthesis, *Landscape Ecology*, 17(4):355–365.

Wu, J., and Y. Qi, 2000. Dealing with scale in landscape analysis: An overview, *Geographic Information Sciences*, 6(1):1–5.

Wu J., E.J. Dennis, L. Matt, and T.T. Paul, 2000. Multiscale analysis of landscape heterogeneity: scale variance and pattern metrics, *Geographic Information Sciences*, 6(1):6–19.

(Received 20 August 2007; accepted 14 November 2007; revised 18 January 2008)